Article

Role of Architecture on Thermorheological Properties of Poly(alkyl methacrylate)-Based Polymers

Bas G. P. van Ravensteijn, Raghida Bou Zerdan, Craig J. Hawker, and Matthew E. Helgeson*

Read Online

ACCESS | 📊 Metrics & More | 📖 Article Recommendations | 🆂🅸 Supporting Information

ABSTRACT: Oil-soluble poly(meth)acrylate-based polymers play a vital role in the thermorheological modification of a wide variety of lubricants and formulated consumer products, where increased viscosity at elevated temperatures ensures sufficient viscosity over a broad temperature range. The assumed mechanism of viscosity modification for many such polymers is based on temperature-induced swelling due to marginal solvent quality. Although this mechanism is widely accepted, direct and consistent experimental proof is limited due to a lack of structural characterization over a wide temperature range. Additionally, the effect of polymer architecture on the temperature-dependent solution behavior is not fully understood, despite the trend toward branched polymers in recent years. Here, we provide a comprehensive set of data relying on detailed temperature-dependent viscosity measurements, dynamic light scattering (DLS), and small-angle neutron scattering (SANS) experiments to confirm the existence of temperature-induced coil expansion for industrially relevant poly(stearyl methacrylate-*co*-methyl methacrylate) (p(SMA-*co*-MMA)) polymers with various architectures including linear, randomly branched, and star-shaped topologies. Compared to the linear and randomly branched polymers, the degree of coil expansion for the star-shaped additives is significantly lower. Regardless of the polymer architecture, the propensity to undergo temperature-induced chain swelling proved to be highly specific toward the type of base oil, underlining the sensitive interplay between polymer and oil chemistry required for designing successful thermorheological modifiers.

Impact of Polymer Architecture
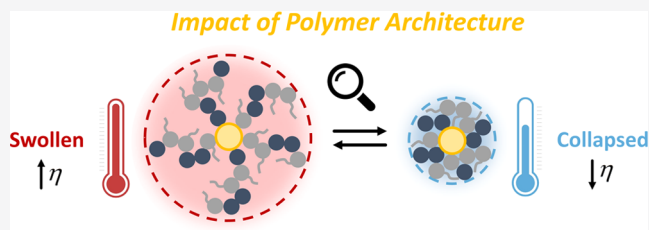
INTRODUCTION

Lipophilic polymers are widely used to tune the physical characteristics of formulated industrial and consumer oil-based products. For example, commercial lubricants contain formulations of polymeric additives in a base oil to perform a wide variety of functions, e.g., friction reduction, protection against wear, foaming and oxidation, and rheological modification, to safeguard lubricant performance and longevity.[1−5] Among these functions, additives that modify the thermal rheology characteristics of oils have received significant attention from both an industrial and an academic perspective. Typically, this class of polymers counteracts the strong decrease in the base oil's viscosity upon increasing temperature, thereby broadening the temperature window in which the formulated oils can be used. Ideally, the action of these rheological modifiers is limited to high temperatures only. In the case of (automotive) lubricants successful thermorheological modifiers combine high load-bearing characteristics at elevated temperatures with conditions that facilitate cold engine start-up.[2] These requirements of successful thermorheological modifiers are schematically depicted in Figure 1a,b.

To date, a large number of polymeric thermorheological modifiers have been reported for oil-based media. The majority of these polymers are based on poly(meth)acrylates, olefin copolymers, and (hydrogenated) poly(styrene-*co*-dienes) with varying architectures.[1,2,5−11] However, the physical mechanism underlying their action has been the topic of debate for decades, with this lack of fundamental understanding hampering the rational design of next-generation rheological modifiers. A commonly accepted mechanism that was first proposed in the late 1950s by Selby et al. relies on a reversible, temperature-induced coil expansion.[12] The expanded polymers provide a greater contribution to the solution viscosity (η) compared to their collapsed-state analogues at low temperature through increased intrinsic viscosity ($[\eta]$), which scales with the coil volume in solution. Since then, only a limited number of studies have been conducted to (directly) validate and prove the temperature-dependent mechanism of successful viscosity-improving polymers. Some of the most comprehensive attempts include the work by Covitch et al.[13] and Bhattacharya et al.,[14] where a combination of scattering and viscosity measurements was performed to probe the temperature-dependent solution behavior of viscosity-improving polymers.
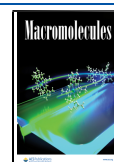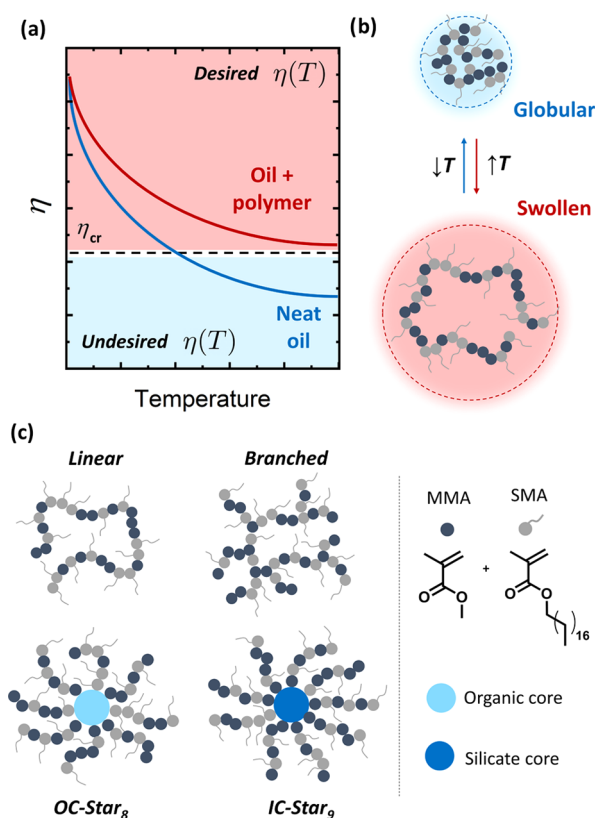
Figure 1. (a) Schematic representation of the thermorheological action of oil-soluble viscosity-modifying polymers. Upon the addition of polymer (red curve), the decrease in viscosity (η) of the pure base oil (blue curve) is weakened. The weaker dependence of η on temperature ensures that the viscosity maintains above a critical threshold (η_{cr}), broadening the temperature window in which the formulated oil can be used, for example, for load-bearing demanding applications found in (automotive) engine environments. (b) Anticipated mechanism underlying the thermorheological performance of some polymeric additives. At low temperatures (blue), the polymers adapt a globular conformation. Increasing the temperature enhances the solvent quality of the base oil for the polymer leading to a coil expansion (red). The swollen coils contribute significantly more to the solution viscosity, thereby counteracting the pronounced natural thinning effect observed for pure base oils (panel a, blue curve). (c) Schematic representations of the employed poly(stearyl methacrylate-*co*-methyl methacrylate) (p(SMA-*co*-MMA))-derived polymers used in this study. The organic star polymers (OC-Star$_8$) contain eight arms attached to a tripentaerythritol core (light blue circle). The inorganic stars (IC-Star$_9$) are based on a hyper-cross-linked silicate core (dark blue circle).

Owing to the high dispersity of the employed polymers and inconsistent results between the individual analytical techniques, conclusive testing of the mechanism(s) responsible for thermorheological modification remains an open challenge.

More recently, there has been considerable work to explore the potential for polymer chain architecture to influence and enhance the rheological properties of polymer solutions. Although linear chains provide the largest change in effective volume and therefore intrinsic viscosity with changes in solvent interactions, researchers have found that branched architectures, including randomly branched, star-like, and dendritic structures,[10,15−23] provide a compromise between viscosity improvement and other deleterious characteristics of linear chains, including their tendency for mechanical scission

encountered in numerous processing and/or application environments. The enhanced resilience against mechanical degradation for nonlinear polymer architectures was confirmed by simulations[17,18] and model polymers in well-controlled flow environments.[15,16] Lower degrees of deformation under shear and relaxation of shear-induced forces via tank-treading and tumbling were identified to originate this behavior. Hyper-branched and star-shaped additives with application-relevant chemistries were synthesized in an attempt to translate these model systems to actual viscosity-improving systems.[10,11,20,21] Although in general these studies confirm the enhanced shear stability of branched architectures, detailed structure−performance relationships and fundamental understanding of the mechanisms underlying their temperature-dependent behavior are often obscured by molecular weight and polydispersity effects. Specifically, it is unclear how the effects of temperature-induced chain swelling differ between linear and more complex architectures, such that no rational guidelines exist to design thermorheological properties of architecturally complex polymers.

Here, we address this shortcoming in fundamental understanding of the physical mechanism underlying thermorheological modification, and its dependence on polymer architecture, by conducting a detailed investigation into the solution behavior of a library of well-defined thermorheological modifiers from commercially available starting materials. Using a combination of viscometry, rheology, dynamic light scattering (DLS), and small-angle neutron scattering (SANS), we probe both the temperature-dependent molecular-scale conformational changes of model thermorheological modifiers and the influence of these changes on macroscopic viscosity behavior. The tested polymers are based on industrially relevant lubricant additives and comprise statistical copolymers of stearyl methacrylate (SMA) and methyl methacrylate (MMA). In-house synthesized linear and star-shaped macromolecules were compared to a commercially available randomly branched polymer (Figure 1c). This set was analyzed to investigate the effect of polymer architecture, and the related propensity to undergo temperature-induced chain swelling, on the ability to alter the thermorheological properties of (model) base oils. Whereas previous studies involved investigations of relatively high-dispersity polymers (Đ > 2.2), the present study relied on a library of well-defined, low-dispersity model polymers. Doing so is instrumental when elucidating the dilute solution behavior as it minimizes the obscuring effects of polydispersity and variations in (hydrodynamic) dimensions on measuring coil dimensions and temperature-dependent solvent qualities.

The results provide a comprehensive study probing the role of temperature-induced coil expansion as an essential mechanism for a successful thermorheological modification. Ultimately, we demonstrate that the swelling propensity is, however, not universal and depends on the type of base oil and polymer architecture, potentially explaining the debate in the existing literature concerning structure/performance relationships for thermorheological modifiers.

■ MATERIALS AND EXPERIMENTAL METHODS

Polymers and Base Oils. A detailed description of the synthetic strategies and characterization of the employed polymers (Figure 1c) was reported previously.[22,24] Relevant physical parameters of the employed polymers are listed in the Supporting Information, Table S1. The employed additives are based on statistical copolymers of

stearyl methacrylate (SMA) and methyl methacrylate (MMA). Polymers with a linear (linear p(SMA-*co*-MMA)) or star-shaped topology were prepared using ruthenium-catalyzed atom transfer radical polymerization (Ru-ATRP).[22] Eight-armed organic stars (OC-Star$_8$) and hybrid organic−inorganic stars having nine (IC-Star$_9$) arms were prepared. The organic stars contained a tripentaerythritol-based core, while the hybrid stars carry an inorganic hyperbranched silicon-containing construct as the core material. These inorganic cores were kindly provided by the Mitsubishi Chemical Corporation (MCC). As a consequence of the selected ATRP polymerization mechanism and choice of initiating moieties, the well-defined linear polymers and the individual arms of the star polymers were end-capped with alkyl bromides. The topologically well-defined polymers obtained using Ru-ATRP were compared to an industrial benchmark additive (branched p(SMA-*co*-MMA), provided by MCC) based on the same monomer repeat units but prepared via suspension-based free-radical polymerization, resulting in a non-negligible degree of random branching. 1-Dodecanethiol was employed as a chain transfer agent, resulting in polymer chains primarily end-capped with dodecyl fragments. The library was synthesized targeting polymers with comparable coil dimensions, as it is hypothesized that this parameter is decisive for determining their thermorheological performance. Radii of gyration (R_g) between 8 and 11 nm were measured using size exclusion chromatography-multiangle light scattering (SEC-MALS; Table S1 and Supporting Information S2). Considering the differences in the macromolecular architecture, the variations in absolute molecular weight were larger within the set of used polymers (70−230 kg mol^{-1}).

To evaluate their thermorheological performance, these polymers were dissolved in either *n*-hexadecane (HD, Sigma-Aldrich, ≥99%) as model oil or in additive-free automotive group III base oils (Yubase 4, YB4 or Nexbase 3043, NB3043) at concentrations ranging from 1 to 3 wt %. These concentrations are inspired by typical additive loadings found in fully formulated oils. *n*-Hexadecane-d$_{34}$ (*d*-HD, 98%) for small-angle neutron scattering (SANS) measurements was obtained from Cambridge Isotope Laboratories. Polymer dissolution in all solvents was aided by sonication and/or moderate heating.

Intrinsic Viscosity Determination. The intrinsic viscosity ($[\eta]$) expresses the relative viscosity increment due to the addition of individual polymer molecules and is often used as a measure for the effective coil volume or radius (R) of polymers with molecular weight, M, as dictated by the Fox−Flory equation[25]

$$[\eta] \sim \frac{R^3}{M} \tag{1}$$

In a dilute polymer solution, the contributions of the polymer coils to the solution viscosity (η) are additive. Therefore, η increases linearly above the solvent viscosity (η_s) with polymer concentration (c). In this dilute limit, η can be written as a virial expansion with the Huggins coefficient (k_H) as the second virial coefficient for the viscosity[25]

$$\eta = \eta_s(1 + [\eta]c + k_H[\eta]^2 c^2 + \cdots) \tag{2}$$

Rearranging the expansion yields either the Huggins (eq 3a) or Kraemer (eq 3b) equation

$$\frac{\eta - \eta_s}{\eta_s c} = [\eta] + k_H[\eta]^2 + \cdots \tag{3a}$$

$$\frac{\ln \eta - \eta_s}{c} = [\eta] + \left(k_H - \frac{1}{2}\right)[\eta]^2 c + \cdots \tag{3b}$$

To determine $[\eta]$, η_s was measured at various polymer concentrations at a fixed temperature (T). Plotting the left-hand side of eqs 3a and 3b against c and extrapolation to zero concentration yields an intercept equal to $[\eta]$. Since $[\eta]$ is an intrinsic property of the polymer coils, both extrapolations should theoretically give identical results.

The temperature dependence of $[\eta]$ was determined by repeating the aforementioned measurement protocol at various temperatures from 25 to 90 °C. The slope of a plot of $[\eta]$ vs T ($[\eta](T)$) was used

as a measure for the propensity of the polymers to swell upon increasing the temperature.

η and η_s required as input for eqs 3a and 3b were measured using an Anton Paar Lovis 2000M rolling ball microviscometer equipped with a temperature-controlled jacket. A 1.50 mm steel ball in either a 1.59 or 1.80 mm glass capillary was used for the viscosity ranges measured in this study. The dimensions of the employed diameter depended on the viscosity of the sample at the set temperature (1.59 = HD samples over the whole temperature range, YB4 and NB3043 samples for temperatures ≥ 50 °C; 1.80 mm = YB4 and NB3043 samples for temperatures ≤ 40 °C). The rolling times of the ball were measured over a distance of 25 mm at an inclination angle of 50° (HD samples) or 30° (YB4, NB3043 samples) for the 1.59 mm capillary and 30° for the 1.80 mm capillary. Measurements were performed at 25, 40, 50, 65, 75, and 90 °C. The values for η and η_s were averaged over at least 10 individual measurements. Extrapolations were performed using a standard least-squares fit.

Viscosity Index (VI) Determination. Based on the standard ASTM D2270 measurement protocol used to benchmark the temperature-dependent viscosity performance of (polymer) additives, viscosity indices (VIs) of YB4-based solutions containing 1 and 2 wt % of the described polymers were determined using[26]

$$\text{VI} = \frac{10^N - 1}{0.00715} + 100 \tag{4}$$

where N is defined as

$$N = \frac{\log(H) - \log(U)}{\log(Y)} + 100 \tag{5}$$

Here, Y and U are the kinematic viscosities (ν) of the solution whose VI is to be calculated in mm^2 s^{-1} at 100 and 40 °C, respectively. H equals ν at 40 °C of a reference oil with VI = 100 that has the same ν at 100 °C as the solution whose VI is to be calculated. H is obtained from an ASTM reference table,[16] while Y and U are measured experimentally.

To this end, dynamic viscosities (η) were determined using an Anton Paar MRC-702 rheometer equipped with a CTD-180 convection oven and a dual-motor configuration that allows variable rotation of the top and bottom geometries. A concentric cylinder (inner diameter = 19.995 mm, outer diameter = 22.000 mm) Taylor−Couette geometry with a gap of 1 mm was used and operated in the outer cylinder rotation mode to prevent the emergence of Taylor−Couette instabilities at elevated shear rates.[27] The samples were equilibrated for 10 min with a temperature tolerance of ±0.1 °C. Steady-state shear rate sweeps between 0.1 and 750 s^{-1} were subsequently performed for all samples. The sweeps were carried out in both directions of increasing and decreasing shear rates, and no significant hysteresis was observed. For calculation of the VI, zero-shear rate viscosities (η_0) were used, which were obtained by extrapolating the shear rate-dependent viscosity data to zero-shear rate. This procedure minimizes the influence of the residual inertial torque of the instrument as evident from a minor slope in the viscosity vs shear rate curves and allows for a consistent comparison between the samples. The obtained zero-shear dynamic viscosities (η_0) were subsequently converted to zero-shear rate kinematic viscosities (ν_0) by dividing with the solution density determined using an Anton Paar DMA 4100 densitometer.

Dynamic Light Scattering (DLS). DLS measurements were performed using a BI-200SM multiangle detector system (Brookhaven Instruments) equipped with a Cobolt Samba 500 mW continuous-wave diode-pumped laser (λ = 532 nm). The applied laser intensity was modulated by passing the laser through an optical neutral density filter (1, 10, 20, 50, or 100% transparency). The type of filter and detector pinhole size were chosen such that the average count rate during measurement was 150−500 kcps. Measurements were performed at a fixed detector angle of 90° and in a temperature range from 25 to 75 °C. Temperature control was provided by an externally connected circulating ethylene glycol/water bath (±0.5 °C precision). Dilute polymer solutions (1.25−10 mg mL^{-1} in HD or
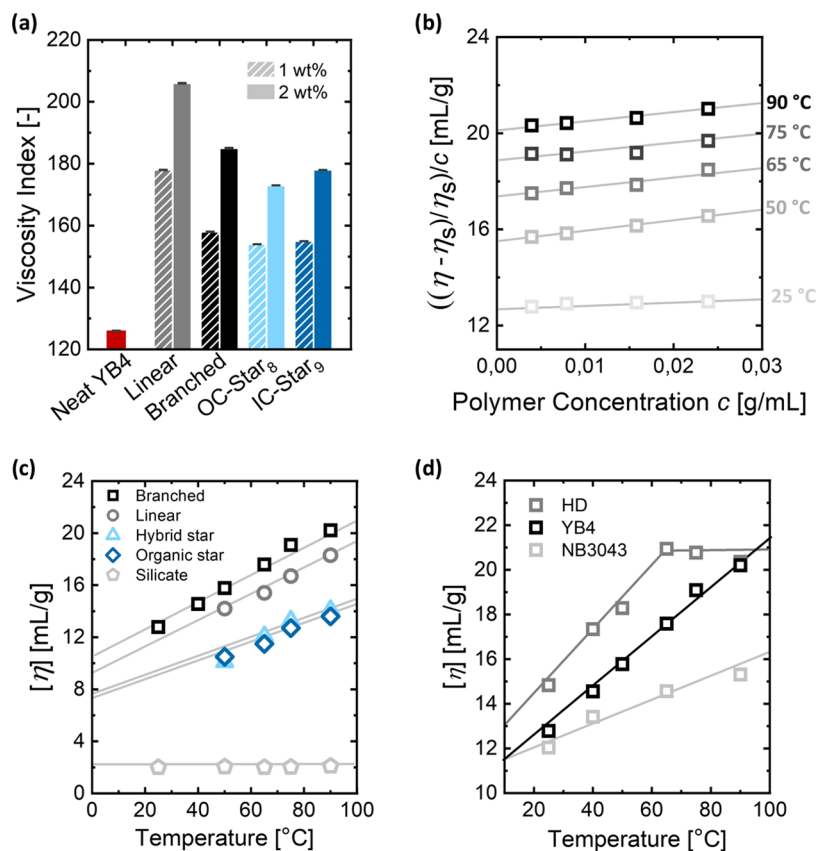
Figure 2. (a) Viscosity indices (VIs) determined for pure Yubase 4 (YB4, red) and its solutions containing poly(stearyl methacrylate-*co*-methyl methacrylate) (p(SMA-*co*-MMA))-derived additives. Gray: linear p(SMA-*co*-MMA), black: branched p(SMA-*co*-MMA), light blue: organic stars carrying eight arms (OC-Star$_8$), dark blue: hybrid stars carrying an average of nine arms (IC-Star$_9$). The striped and solid columns represent solutions containing 1 and 2 wt % of polymer, respectively. (b) Huggins plots of branched p(SMA-*co*-MMA) as a function of temperature. (c) Intrinsic viscosities ($[\eta]$) as a function of temperature for the p(SMA-*co*-MMA)-based additives. To emphasize that the increase in $[\eta]$ is caused by swelling of the polymers, data for a rigid silicate additive are included (light gray diamonds). The absence of any temperature-induced swelling manifests itself by a constant $[\eta]$ over the probed temperature window. (d) $[\eta]$ for branched p(SMA-*co*-MMA) as a function of temperature in YB4 (black), Nexbase 3043 (NB3043, light gray), and *n*-hexadecane (HD, dark gray).

YB4) were passed through a 0.45 μm Teflon syringe filter into the glass sample tube immediately before the measurement. The autocorrelation functions ($G_1(\tau)$) reported here decay from 1 at short delay times (τ) to 0 at long delay times. To facilitate direct comparison between the individual scattering experiments performed at different temperatures, $G_1(\tau)$ is plotted as a function of the reduced delay time t', which is the measured delay time τ multiplied by the temperature (T) and divided by the viscosity (η) of the dispersing medium (eq 6)[28,29]

$$t' = \frac{\tau T}{\eta} \tag{6}$$

η was measured using the rolling ball microviscometer. The autocorrelation functions were converted to intensity-weighted hydrodynamic size distributions using a cumulant method.

Small-Angle Neutron Scattering (SANS). SANS measurements were performed at the NIST Center for Neutron Research on the NGB 30 m SANS instrument. The scattering vector q is defined as $q = 4\pi \sin(\theta/2)/\lambda$, where θ is the angle at which the neutron is scattered and λ is the neutron wavelength. Data were collected at four detector configurations to span the desired q range (0.003−0.4 Å^{-1}) using a wavelength of $\lambda = 8.4$ Å^{-1} and $\Delta\lambda/\lambda = 0.125$ at a sample-to-detector distance of 30 m and a wavelength of $\lambda = 6$ Å^{-1} and $\Delta\lambda/\lambda = 0.125$ at sample-to-detector distances of 1.3, 4, and 13.2 m. The samples, 3 wt % solutions of p(SMA-*co*-MMA)-based polymers in *n*-hexadecane-d$_{34}$ (*d*-HD), were loaded into 1 mm thick titanium scattering cells sandwiched between two quartz windows for SANS measurement. Measurements at 25, 50, 75, and 90 °C were performed. The

temperature was controlled with a circulating glycol bath, and a thermal equilibration time of 15 min was used before data acquisition. SANS data were reduced using the NCNR IGOR software package[30] and analyzed using the SasView software package.[31] The temperature-dependent radii of gyration (R_g) of the linear and star-shaped p(SMA-*co*-MMA) polymers were determined using a model-free Guinier analysis of the scattering profiles. To this end, the natural logarithm of the scattered intensity ($I(q)$) was plotted against q^2. Following the Guinier formalism, the slope of a linear fit in the low q regime equals $R_g^2/3$ and gives therefore direct access to the dimensions of individual polymer chains.[32] For the branched p(SMA-*co*-MMA) derivatives, sufficient linearization of the scattering spectrum at low q values was not achieved. In this case, R_g was determined by fitting the scattered profiles to a model describing the scattering of polymer chains with excluded volume interactions (see the Supporting Information S7 for details).[33]

■ RESULTS AND DISCUSSION

Polymer Library Design. As depicted in Figure 1c, the set of p(SMA-*co*-MMA)-based polymers evaluated in this study comprises a truly linear, a randomly branched, and two star-shaped macromolecules. This library was constructed such that polymers have varying architecture, but approximately equal hydrodynamic dimensions were obtained (see Supporting Information S1). By tailoring the molecular weight of the synthesized linear and star-shaped polymers, the dimensions of
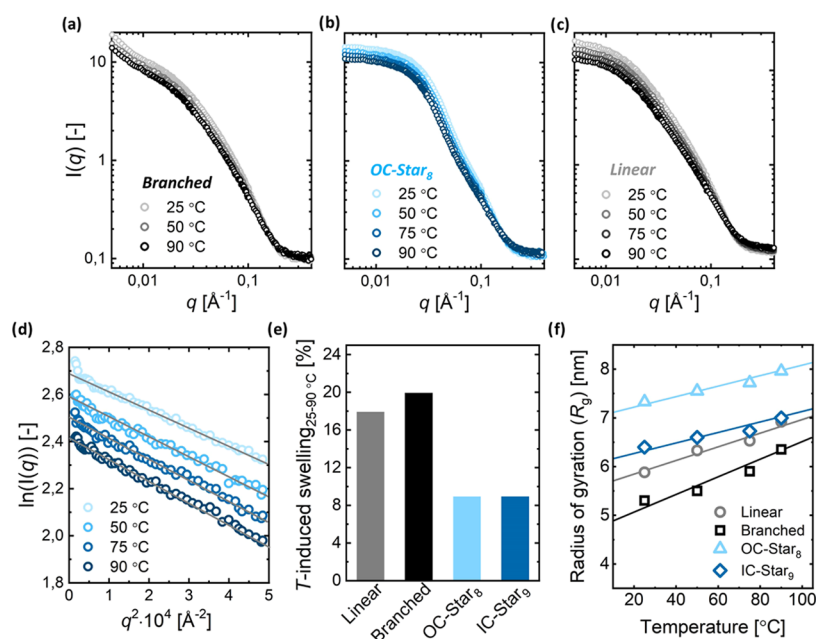
Figure 3. Small-angle neutron scattering (SANS) profiles as a function of temperature for (a) branched, (b) organic star-shaped, and (c) linear poly(stearyl methacrylate-*co*-methyl methacrylate) (p(SMA-*co*-MMA)) additives. (d) Guinier analysis for scattering profiles shown in panel (b). (e) Percentage of temperature-induced chain swelling between 25 and 90 °C derived from the radii of gyration (R_g). (f) Plot of R_g vs temperature. Gray: linear p(SMA-*co*-MMA), black: branched p(SMA-*co*-MMA), light blue: organic stars carrying eight arms (OC-Star$_8$), dark blue: hybrid stars carrying an average of nine arms (IC-Star$_9$).

the supplied randomly branched additive could be matched. By keeping the coil dimensions fixed, the effect of branching on the anticipated thermoresponsive behavior can be assessed independently of changes in molecular volume that would be accompanied by alternatively studying a library where the molecular weight remains constant across the different architectures.

Viscosity Index (VI) Improvement. As prerequisite to study the mechanism behind thermorheological modification is the need for polymeric additives that convincingly fulfill this task. To this end, we first evaluated the viscosity-improving capacity of the p(SMA-*co*-MMA)-based additives by measuring the viscosity index (VI) of dilute polymer solutions using a commercial base oil (Yubase 4, YB4) as solvent. The VI is an industrially applied dimensionless performance indicator that quantifies the temperature sensitivity of a solution's viscosity over a temperature range from 40 to 100 °C (see the Viscosity Index (VI) Determination section for details). The sensitivity is inversely related to the value of the VI. Therefore, high VI values correspond to solutions with viscosities that remain more constant upon an increase in temperature (Figure 1, red curve).

VI measurements for the complete architectural library of p(SMA-*co*-MMA) additives in YB4 (Figure 2a) demonstrate that, regardless of the branching details of the polymers, an increase in VI was measured compared to that of the neat base oil (Figure 2a, red column). As shown in Supporting Information S3, this increase in VI is caused by a relatively strong enhancement of the solution viscosity at 100 °C, while the viscosity at 40 °C remains little affected by the presence of the additives. As elaborated in the Introduction section and schematically depicted in Figure 1, this is the behavior associated with effective thermorheological-modifying polymers.[2,3,5]

Although the additives show the desired thickening behavior, the physical mechanism driving the VI enhancement cannot be deduced from these measurements. However, indications toward the temperature-induced swelling mechanism can be inferred from the relation between the VI increase (ΔVI) upon the addition of polymers and the effect of their degree of branching. The linear polymers (Figure 2a, gray column) are most efficient in modifying the rheological characteristics of the oil, while highly branched stars (Figure 2a, blue columns) are the least effective. The randomly branched free-radical-derived polymers (Figure 2a, black column) are positioned between these two extreme cases. These measurements suggest that introducing an increasing amount of branching limits the conformational freedom of the polymer to undergo (temperature-induced) coil expansions.[34]

Additionally, for the star-shaped polymers, the individual arms adopt more stretched conformations compared to ideal polymer chains as a consequence of excluded volume interactions with neighboring arms.[34,35] This further limits the volumetric chain expansion that these star polymers can undergo. The validity of these assertions will be tested by the more detailed intrinsic viscosity and scattering measurements to follow.

Temperature Dependence of the Intrinsic Viscosity ([η]). Measurements of the intrinsic viscosity ([η]) and its temperature dependence were used to gain greater insight into the temperature-dependent solution behavior and test the hypothesis that swelling is responsible for the observed increase in VI. At sufficiently low polymer concentration, i.e., well below the overlap concentration (c^*) of the polymeric species of interest, [η] is proportional to the volume of an individual polymer chain (for c^* estimations, see Supporting Information S4). Therefore, by determining [η] for p(SMA-*co*-MMA)-based polymers at different temperatures, the tendency of the coils to swell in response to an increase in temperature

can be assessed. To determine $[\eta]$, detailed viscosity measurements were performed as a function of the polymer concentration (c). Linear relations between the polymer concentration and the solution viscosity (η) were found, indicating that the measurements were performed in the dilute regime. Extrapolating the concentration-dependent viscosity data following the Huggins or Kraemer relations (3a and 3b, respectively) to $c = 0$ yields the intrinsic viscosity at the given measurement temperature. The Huggins extrapolations for the branched additive are shown in Figure 2b and are representative of the data obtained for the other polymers. The results of the Kraemer extrapolations can be found in Supporting Information S5.

Compiling all $[\eta]$'s as a function of temperature for YB4-based polymer solutions yields Figure 2c. In agreement with the previously stated interpretation of $[\eta]$ and the increase in VI upon the addition of these polymers, $[\eta]$ increases upon heating. As a reference, we also measured $[\eta]$ for an additive solely composed of the cross-linked silicate cores used to prepare star polymers (Figure 2c, light gray diamonds). These molecularly rigid cores are not expected to undergo any appreciable swelling, and this behavior is reflected by the invariance of $[\eta]$ with temperature. As anticipated by the topological constraints imposed by the star-shaped architecture, the absolute values of $[\eta]$ and its sensitivity toward changes in temperature, measured by the slope of the $[\eta]$ vs temperature ($\mathrm{d}[\eta]/\mathrm{d}T$), are smallest for these polymers (Figure 2c, blue triangles and squares). Considering the low number of arms per polymer, conformational freedom of the individual arms can explain this significant coil swelling. This is in contrast to previously studied dendritic or hyperbranched polymers.[10,23] These types of macromolecular structures are significantly more rigid, compact, and globular, which hampers coil expansion. By contrast, the polymers with a linear and randomly branched architecture appear to be more expanded entities capable of increasing their coil volume more dramatically (Figure 2c, black squares, gray circles). Despite the lower total molecular weights of these macromolecules compared to those of the stars (see Supporting Information S1), the lack of conformational constraints leads to larger coils. Furthermore, the effect of polydispersity should be considered for the randomly branched additive. The presence of extremely high-molecular-weight impurities (see the Small-Angle Neutron Scattering (SANS) section, Figure 3a) can lead to significant enhancement of the solution viscosity beyond what is expected based on the average molecular weight. Although it was reported before that linear polymers are the most efficient thermorheological modifiers,[22] a large difference in VI between the linear and randomly branched additives was not expected based on the negligible difference in $[\eta]$ and its temperature dependency. We speculate that this behavior is caused by differences in the chain-end chemistries of the linear (ATRP-derived chain end) and branched polymers (initiator/chain transfer agent). Weakly attractive terminal groups might lead to short-lived, transient associations, further increasing the bulk viscosity.[36−38]

In addition to the viscosity measurements in YB4, the temperature dependence of the intrinsic viscosity of the randomly branched additive was determined in an alternative commercial base oil (Nexbase 3043, NB3043) and n-hexadecane (HD) as model oil (Figure 2d). Clearly, the swelling capacity of this polymer derived from these viscosity measurements is highly dependent on the solvent. The

polymer seems more temperature-responsive in HD, while this sensitivity is suppressed in NB3043. Considering the (apparent) absence of any functional groups that can modulate the interaction between the polymers and the purely hydrocarbon solvents, this is a surprising and unexpected observation. The data suggest that universal thermorheological modifiers are most likely not attainable and that careful optimization of the polymer chemistry is required for a specifically targeted base oil. The importance of solvent quality of the polymers in the different oils will be assessed at the end of the Results and Discussion section.

Temperature-Dependent Small-Angle Neutron Scattering (SANS). In addition to the detailed viscosity measurements, SANS experiments were performed on dilute polymer solutions to directly relate temperature-induced changes in coil dimensions to the observed viscosity changes. Perdeuterated n-hexadecane (d-HD) was used as a model oil. Employing a fully deuterated solvent enhances the scattering contrast between the solvent and the polymers of interest, enabling these measurements. Additionally, based on the intrinsic viscosity measurements, swelling is pronounced in this solvent, facilitating the analysis and interpretation of the acquired SANS data. Scattering profiles were recorded for the linear, randomly branched, and star-shaped additives in a temperature range of 25−90 °C (Figure 3). The profiles for the hybrid star copolymers resemble those obtained for their full organic counterparts and can be found in Supporting Information S6. The profiles obtained for the linear and randomly branched polymers show no distinct features (Figures S10 and 3a), as anticipated for these unstructured polymers. The excess scattered intensity in the low q regime observed for the branched polymer indicates the presence of large(r) entities in solution (Figure 3a). This excess scattering is most likely due to larger objects arising from the free-radical-based polymerization employed to synthesize the branched p(SMA-co-MMA) polymers, which yields polymer with a large dispersity and the formation of interconnected polymer chains with (extremely) high molecular weights. These features are suppressed when relying on controlled radical polymerizations as was the case for the remaining polymers employed in this study. The scattering profiles measured for the star-shaped additives show a subtle protuberance at $q \approx 0.1$ Å^{-1} (Figure 3b), which is attributed to the scattering of the interface between the core of these star polymers and their arms.[23,26] The presence of the anticipated star-shaped architecture was further corroborated by an excellent fit of the scattering profiles with models for ideal star polymers (Supporting Information S7). Importantly, the excluded volume parameters (ν) obtained from these fits (Table S5) increase with increasing temperature ($\nu_{25\,°C} = 0.24$; $\nu_{90\,°C} = 0.30$), consistent with an enhancement of the solvent quality at elevated temperatures. This provides an important direct verification of the mechanism of temperature-dependent polymer swelling and therefore the mechanism of viscosity improvement.

Regardless of the polymer topology, the scattered intensity decreases with increasing temperature in the low q range (0.004−0.02 Å^{-1}) regime. As the global polymer concentration is held fixed during the measurements, this decrease can be interpreted as a loss in scattering contrast between the polymer coils and the surrounding solvent. This loss in contrast agrees with the hypothesis that the p(SMA-co-MMA)-based polymers undergo swelling upon heating, as this process is driven by enhanced solvation of the polymer chains. To make this

qualitative indication for temperature-induced swelling more quantitative, the radii of gyration (R_g) as a function of temperature were extracted from the scattering profiles following a Guinier analysis (see the Small-Angle Neutron Scattering (SANS) section for details). To this end, the data in the low q range are plotted as q^2 vs $\ln(I(q))$ and fitted with a linear function, as depicted in Figure 3d for the organic star-shaped polymers (Guinier fits for the other polymers can be found in Supporting Information S6). The value of R_g can then be directly extracted from the slope of these fitted curves. As was noted previously, this analysis could not be performed for the randomly branched polymers since the scattering profiles do not plateau at low q, making any fit to the data in this q regime unreliable. Alternatively, the coil dimensions were determined by fitting the scattering profiles for the branched additives to a model describing the scattering from a polymer with excluded volume interactions (Supporting Information S7). The low q regime ($q < 0.01$) was omitted for this procedure to suppress the influence of the anticipated small fraction of ultrahigh-molecular-weight species. The obtained R_g values are plotted as a function of temperature in Figure 3f. Coil radii on the order of 5−7 nm were found, which are in reasonable agreement with previously reported static light scattering experiments on these polymers in chloroform (see Supporting Information S1).[22] Similar to the star-shaped additives, the excluded volume parameter of the branched additive was found to increase with increasing temperature (Supporting Information S7). The R_g values obtained for the star-shaped additives are larger than the corresponding values obtained for the linear polymer. These small differences in R_g potentially originate from the finite size of the star polymer's core (hydrodynamic radius $\approx 0.75-1$ nm as measured with diffusion ordered spectroscopy (DOSY) NMR) and a nonisotropic distribution of polymer grafting points. Although apparently in conflict with the previously presented viscosity data (Figure 2c), this inconsistency might originate from unaccounted effects of (temperature-dependent) solvent quality and chain architecture in the proportionality constant in the Flory−Fox equation (eq 1) relating coil dimension to intrinsic viscosity.

Nevertheless, all additives undergo a temperature-induced coil expansion upon heating, as reflected by an increase in R_g with increasing temperature. Based on the measured R_g values, the swelling percentages upon heating (S_{SANS}) were calculated according to eq 7

$$S_{SANS} = \frac{R_{g,90} - R_{g,25}}{R_{g,25}} \times 100\% \qquad (7)$$

where $R_{g,25}$ and $R_{g,90}$ are the radii of gyration at 25 and 90 °C, respectively. In agreement with the VI, $[\eta]$ measurements, and polymer topology, the swelling is more pronounced for the linear polymer compared to that of their branched analogues (Figure 3e). No significant distinction in the swelling capacity can be made when comparing the fully organic stars of their hybrid counterparts (Figure 3e, light vs dark blue), consistent with the hypothesis that the increase in R_g is exclusively caused by extension of the p(SMA-*co*-MMA) arms and not the dimensions and chemical details of the employed cores.

Temperature-Dependent Dynamic Light Scattering (DLS). To complement the SANS experiments, light scattering measurements as a function of temperature were performed to determine the hydrodynamic coil dimensions not only in *n*-

hexadecane but also directly in YB4. The measurements were performed at 25, 50, and 75 °C for the complete set of p(SMA-*co*-MMA)-based polymers. The data obtained for the organic star polymer and the randomly branched additive are depicted in Figure 4 and are representative for all macromolecules (see
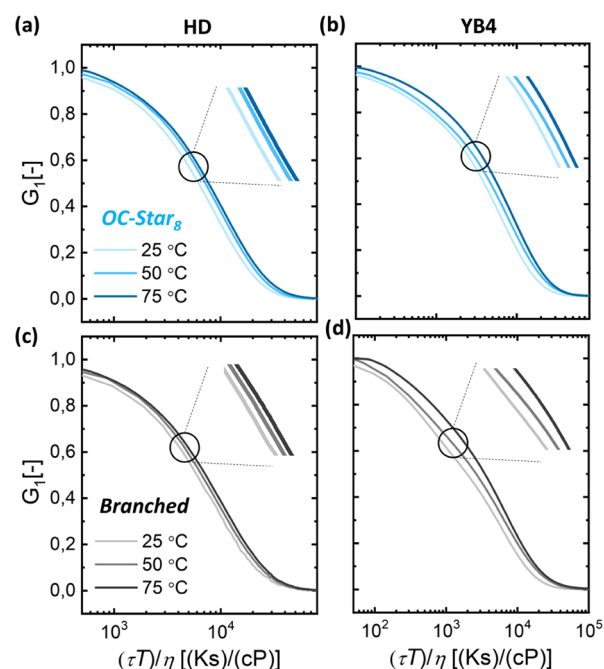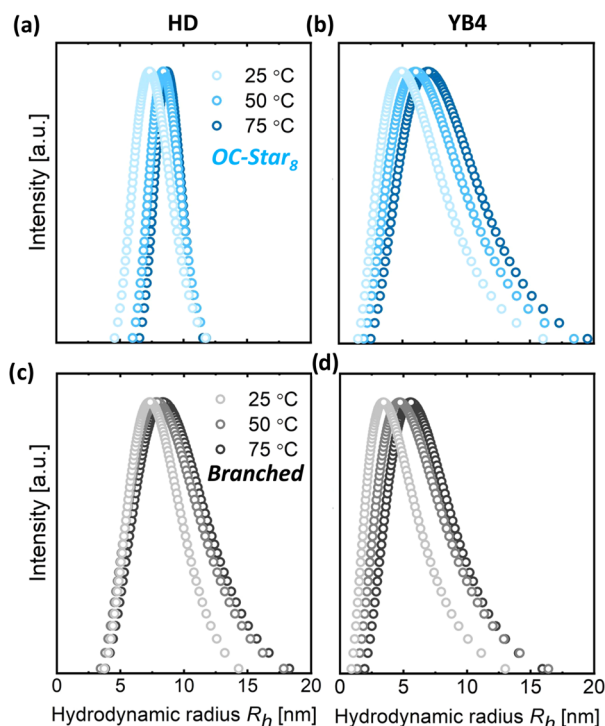

Figure 4. Normalized correlation functions (G_1) as a function of temperature obtained using dynamic light scattering (DLS) for poly(stearyl methacrylate-*co*-methyl methacrylate) (p(SMA-*co*-MMA)) organic star polymers (OC-Star$_8$) in (a) *n*-hexadecane (HD) and (b) Yubase 4 (YB4). DLS correlation functions of branched p(SMA-*co*-MMA) in (c) HD and (d) YB4. The inset shows the shift of the correlation functions to longer characteristic decay times upon increasing the temperature, which is evidence for coil expansion.

Supporting Information S8). Polymer concentrations of 10 mg mL^{-1} were used to account for the low scattering intensity of the polymers in YB4 solutions (see Supporting Information S9). As these polymer concentrations are still below the estimated overlap concentration, the DLS-derived sizes should correspond to those of single polymer chains. Experimentally, this was confirmed by performing DLS measurements on HD-based samples with polymer concentrations varying between 1.25 and 10 mg mL^{-1}. The obtained correlation functions and derived size distributions proved to be independent of concentration within this window, confirming that the data were collected in the dilute regime (Supporting Information S10).

For all polymers, single-exponential correlation functions were found, indicating low dispersity of the polymers and the absence of large(r) aggregates or impurities. To directly evaluate the effect of temperature on the correlation data, the raw functions were rescaled and plotted against a reduced delay time (t') to account for temperature-induced changes in the viscosity of the dispersing medium. The average size of the scattering objects is reflected by the inflection point of the decay of the correlation function, here referred to as the characteristic decay time (t'_c). An increase in the value of t'_c is associated with objects that, on average, diffuse slower and

hence have larger hydrodynamic dimensions. For the set of polymers studied here, the normalized correlation functions shift to higher values of t' upon increasing the temperature (Figure 4, insets), which implies an increase in hydrodynamic size. This behavior is observed for measurements performed on polymer solutions using HD and YB4 as solvents, further strengthening the claim that coil expansion has to be considered in the specific context of thermorheological modification and associated applications.

To gain more insight into the temperature-induced changes in the hydrodynamic radii of the polymers, the correlation functions were converted to intensity-weighted size distributions (Figure 5). Naturally, the size distributions follow the

Figure 5. Intensity-weighted size distributions measured with dynamic light scattering (DLS) for poly(stearyl methacrylate-*co*-methyl methacrylate) (p(SMA-*co*-MMA)) organic star polymers (OC-Star$_8$) in (a) *n*-hexadecane (HD) and (b) Yubase 4 (YB4). Analogous size distributions for the branched p(SMA-*co*-MMA) in (c) HD and (d) YB4. Distributions of the hydrodynamic radius (R_h) vs intensity were obtained from the correlation functions shown in Figure 4.

same trends as the correlation function in that the distribution shifts to larger sizes upon heating. In HD, the average hydrodynamic radii as measured with DLS are in close agreement with the average values of R_g determined by SANS, emphasizing the internal consistency of the different analytical techniques used in this work. Additionally, the spread in hydrodynamic sizes for the individual polymers is comparable to the variations in R_g, as determined with SEC-MALS (see Supporting Information S2).

Calculating the swelling percentages (S_{DLS}) between 25 and 75 °C from hydrodynamic radii using a relation analogous to eq 7 reveals similar trends. Specifically, we find that the linear and branched additives swell more compared to their star-shaped counterparts (Figure 6). For this calculation, the maxima of the DLS size distributions were used, as the shape
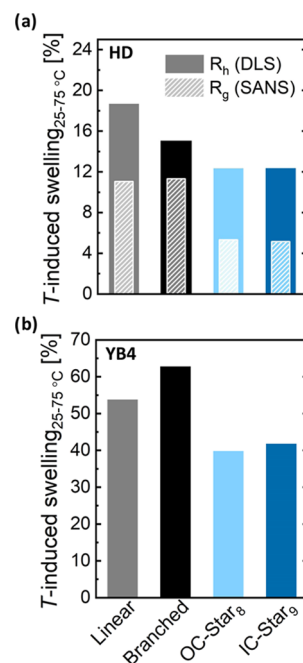
Figure 6. Percentage of temperature-induced chain swelling of p(SMA-*co*-MMA)-based thermorheological modifiers between 25 and 75 °C in (a) *n*-hexadecane (HD) and (b) Yubase 4 (YB4). The filled columns represent swelling percentages derived from hydrodynamic radii (R_h), while the data represented by the stripped columns in panel (a) are based on radii of gyration (R_g). (b) Gray: linear p(SMA-*co*-MMA), black: branched p(SMA-*co*-MMA), light blue: organic stars carrying eight arms (OC-Star$_8$), dark blue: hybrid stars carrying an average of nine arms (IC-Star$_9$).

of the size distributions remained unaffected upon increasing the temperature. S_{DLS} for protonated HD-based solutions is larger than the swelling percentage derived from SANS measurements in deuterated HD (S_{SANS}) (Figure 6a, filled vs stripped columns). This is potentially related to differences between hydrodynamic radii and radii of gyration and their temperature dependence. Additionally, subtle isotopic effects caused by substituting all hydrogens for deuterium atoms in the base oil may affect the solution behavior. Interestingly, S_{DLS} for polymer solutions using YB4 as solvent are significantly higher compared to their HD counterparts (Figure 6). This effect is mainly attributed to the more collapsed initial coil conformation at low temperatures (Figure 5a vs b and c vs d), giving the polymers more freedom to expand upon increasing the temperature. The enhanced swelling capability in YB4 seems in conflict with the absolute values and temperature dependence of $[\eta]$, where the polymers displayed the strongest coil expansion in HD-based solutions (Figure 2d). We speculate that this apparent internal inconsistency is related to the previously mentioned unaccounted solvent quality and architectural effects on the proportionality constant in the Flory–Fox equation (eq 1).

Comparing the size distributions obtained for HD- and YB4-based solutions (Figure 5) reveals that the distributions in the commercial base oil are significantly broader and tail to larger dimensions. This behavior is strikingly illustrated in Figure 5b for the organic star polymers. As these polymers were synthesized using controlled radical polymerizations, these polymers are uniform in their molecular weight and hence coil dimensions, as reflected by the relatively narrow and

symmetrical R_h distributions when dissolved in HD. In YB4, highly unsymmetrical distributions with tails corresponding to species with larger hydrodynamic radii were obtained. Additionally, the polymers appear more collapsed in the commercial base oil compared to those in the HD model oil. These two observations can be rationalized by considering the solvent quality of HD vs YB4 for these p(SMA-co-MMA)-based polymers. More compact coils are formed when the oil is not able to solvate the polymers efficiently. Using poor or marginally good solvents can also enhance the tendency toward (weak) aggregation, which results in the (transient) formation of entities with larger hydrodynamic radii. In view of the application of these polymers as thermorheological modifiers, it can be argued that this behavior is beneficial. The compacter coils at low temperatures have more conformational freedom to undergo expansion, generating a greater driving force to counteract the natural thinning effect of the base oil while at the same time minimizing the effect of the polymers on the solution viscosity increase at low temperatures (Figure 1). Furthermore, the larger polymer aggregates are more effective in increasing the viscosity of the oil compared to their individual analogues, further enhancing the rheological signature of the polymers.

In addition to the benefits of using poorly solubilized polymers, relying on weak aggregates of the additives instead of molecularly dissolved polymers with higher molecular weights, and hence coil sizes, has the advantage that the system as a whole becomes more resilient against mechanical degradation under the high-shear environments encountered in real-life (automotive) applications. High-molecular-weight polymers are prone to irreversible bond scission under high shear.[15,16] As the viscosity-improving power sensitively depends on the coil dimensions of the polymers, this chain breakage leads to a detrimental drop in thickening performance. In contrast, clusters of lower-molecular-weight (weakly) aggregating polymers can reform after the high-shear conditions are removed, as only suprapolymeric bonds are broken.

CONCLUSIONS

In this work, we present a consistent set of experimental data confirming temperature-induced polymer swelling as the mechanism of thermorheological modification for an architectural library of p(SMA-co-MMA)-based polymers in model base oils for commercial formulations. The swelling was probed using detailed viscosity measurements and corroborated with direct determinations of the radius of gyration and hydrodynamic radius as a function of temperature, using SANS and DLS, respectively. Importantly, changes in solvent quality as the mechanism for temperature-induced swelling were confirmed by detailed modeling of SANS data to extract the excluded volume parameter of individual chains. Based on the presented experimental results, the successful design of effective thermorheological modifiers requires careful optimization of the (temperature-dependent) solvent quality of the targeted base oil. In addition to the increase in solvent quality upon heating that drives coil swelling, observed regardless of the polymer topology, the presented data suggest that the polymer chemistry of successful viscosity modifiers needs to be tuned such that the targeted base oil is a moderately good solvent for the polymer. This ensures that the polymeric coils are relatively compact at low temperatures, providing sufficient room for swelling. Additionally, this promotes the formation of weak polymer associations that act as high-molecular-weight

species to further boost the thickening power. This behavior could explain the previously observed relative high-shear stability of some poly(meth)acrylate-based polymers, as such weak clusters can dynamically break and reform to dissipate molecular tension.[39,40] These insights offer new design parameters for high-performance thermorheological polymer additives. For example, dedicated (supra)molecular moieties that would enhance this transient clustering behavior could be incorporated. Strategies along similar lines were previously reported for aqueous associative thickeners[36−38] and supramolecular polymers.[41,42] Systematic studies into the effects of the number and nature of the end groups and their associated attractive strength are therefore recommended for future research.

By comparing relatively monodisperse polymeric additives with comparable coil dimensions, the effect of chain architecture on the temperature-dependent solution behavior could be unraveled. In agreement with previous (simulation) reports, the degree of coil expansion is less for star-shaped polymers compared to that of their more linear analogues. Therefore, at zero shear, more linear polymers outcompete branched architectures in terms of thermorheological modification. However, coil size only is not sufficient to predict viscosity-improving performance. Comparing the truly linear polymers with the star-shaped polymers reveals a moderate decrease of approximately 15% in VI, while DLS and SANS gave a 40−50% reduction in relative swelling capability. Together with the experimental observation that low-dispersity star polymers show broad and tailing size distributions in base oils, we hypothesize that the relatively pronounced ability to modify the rheological characteristics of these star polymers is caused by more efficient interpolymer attractions mediated by a high concentration of more exposed end groups. Future studies might focus on how to fully leverage the topological placement of associative moieties to simultaneously maximize zero-shear viscosity improvements and high-shear resilience.

Finally, as the degree of chain swelling with increasing temperature was found to be sensitive to the type of base oil, the presented results imply that the design of a universal thermorheological modifier for the wide variety of available base oils is challenging, potentially explaining the inconsistencies on the mechanism behind viscosity improvement in the current literature. Future studies toward the rational design of next-generation viscosity improvers should therefore focus on investigating (temperature-dependent) polymer−solvent interactions in the context of the specific formulations in which they are applied.

ASSOCIATED CONTENT

ⓈI Supporting Information

The Supporting Information is available free of charge at https://pubs.acs.org/doi/10.1021/acs.macromol.1c00149.

> Overview of employed p(SMA-co-MMA)-based thermorheological modifiers; size exclusion chromatography-multiangle light scattering analysis; viscosity data used for calculation of the VI; estimation of overlap concentration c^* for the p(SMA-co-MMA) additives; Kraemer extrapolations of viscosity data to determine intrinsic viscosities $[\eta]$; SANS profiles for linear p(SMA-co-MMA) and IC-Star$_9$; Guinier and fitting analysis for linear, branched p(SMA-co-MMA), and IC-Star$_9$; DLS data for linear p(SMA-co-MMA) and IC-Star$_9$; scattered

intensity in DLS: HD vs YB4 as solvent; and concentration dependence of DLS correlation functions and size distributions (PDF)

(PDF)

AUTHOR INFORMATION

Corresponding Author

Matthew E. Helgeson − *Department of Chemical Engineering, University of California, Santa Barbara, California 93106, United States;* ⊙ orcid.org/0000-0001-9384-4023; Email: helgeson@engineering.ucsb.edu

Authors

Bas G. P. van Ravensteijn − *Department of Chemical Engineering and Materials Research Laboratory, University of California, Santa Barbara, California 93106, United States;* Present Address: Institute for Complex Molecular Systems, Department of Chemical Engineering and Chemistry, Eindhoven University of Technology, P.O. Box 513, 5600 MB, Eindhoven, The Netherlands.; ⊙ orcid.org/0000-0001-9024-3927

Raghida Bou Zerdan − *Materials Research Laboratory, University of California, Santa Barbara, California 93106, United States;* Present Address: Dow Performance Silicones, The Dow Chemical Company, Midland, Michigan 48667, United States.; ⊙ orcid.org/0000-0002-5361-5565

Craig J. Hawker − *Department of Chemistry and Biochemistry and Materials Department, University of California, Santa Barbara, California 93106, United States;* ⊙ orcid.org/0000-0001-9951-851X

Complete contact information is available at:
https://pubs.acs.org/10.1021/acs.macromol.1c00149

Author Contributions

The manuscript was written through contributions of all authors. All authors have given approval to the final version of the manuscript.

Notes

The authors declare no competing financial interest.

REFERENCES

(1) Rudnick, L. R. *Lubricant Additives - Chemistry and Applications,* 2nd ed.; Kinker, B. G., Ed.; CRC Press: Boca Raton, 2009; pp 283−337.

(2) Ver Strate, G.; Stuglinski, M. J. Polymers as Lubricating-Oil Viscosity Modifiers. *ACS Symp. Ser.* **1991**, *462*, 256−272.

(3) Rizvi, S. Q. A. A. *A Comprehensive Review of Lubricant Chemistry, Technology, Selection and Design*; ASTM International: West Conshohocken, 2009.

(4) Mang, T.; Dresel, W. *Lubricants and Lubrication*, 3rd ed.; John Wiley & Sons, 2017.

(5) Martini, A.; Ramasamy, U. S.; Len, M. Review of Viscosity Modifier Lubricant Additives. *Tribol. Lett.* **2018**, *66*, No. 58.

(6) Mohamad, S. A.; Ahmed, N. S.; Hassanein, S. M.; Rashad, A. M. Investigation of Polyacrylates Copolymers as Lube Oil Viscosity Index Improvers. *J. Pet. Sci. Eng.* **2012**, *100*, 173−177.

(7) Nassar, A. M. The Behavior of Polymers as Viscosity Index Improvers. *Pet. Sci. Technol.* **2008**, *26*, 514−522.

(8) Jordan, E. F.; Smith, S.; Koos, R. E.; Parker, W. E.; Artymyshyn, B.; Wrigley, A. N. Viscosity Index. I. Evaluation of Selected Copolymers Incorporating N-octadecyl Acrylate as Viscosity Index Improvers. *J. Appl. Polym. Sci.* **1978**, *22*, 1509−1528.

(9) Van Horne, W. L. Polymethacrylates as Viscosity Index Improvers and Pour Point Depressants. *Ind. Eng. Chem.* **1949**, *41*, 952−959.

(10) Wang, J.; Ye, Z.; Zhu, S. Topology-Engineered Hyperbranched High-Molecular-Weight Polyethylenes as Lubricant Viscosity-Index Improvers of High Shear Stability. *Ind. Eng. Chem. Res.* **2007**, *46*, 1174−1178.

(11) Robinson, J. W.; Zhou, Y.; Qu, J.; Bays, J. T.; Cosimbescu, L. Highly Branched Polyethylenes as Lubricant Viscosity and Friction Modifiers. *React. Funct. Polym.* **2016**, *109*, 52−55.

(12) Selby, T. W. The Non-Newtonian Characteristics of Lubricating Oils. *ASLE Trans.* **1958**, *1*, 68−81.

(13) Covitch, M. J.; Trickett, K. J. How Polymers Behave as Viscosity Index Improvers in Lubricating Oils. *Adv. Chem. Eng. Sci.* **2015**, *05*, 134−151.

(14) Bhattacharya, P.; Ramasamy, U. S.; Krueger, S.; Robinson, J. W.; Tarasevich, B. J.; Martini, A.; Cosimbescu, L. Trends in Thermoresponsive Behavior of Lipophilic Polymers. *Ind. Eng. Chem. Res.* **2016**, *55*, 12983−12990.

(15) Xue, L.; Agarwal, U. S.; Lemstra, P. J. Shear Degradation Resistance of Star Polymers during Elongational Flow. *Macromolecules* **2005**, *38*, 8825−8832.

(16) Odell, J. A.; Keller, A.; Rabin, Y. Flow-Induced Scission of Isolated Macromolecules. *J. Chem. Phys.* **1988**, *88*, 4022−4028.

(17) Jabbarzadeh, A.; Atkinson, J. D.; Tanner, R. I. Effect of Molecular Shape on Rheological Properties in Molecular Dynamics Simulation of Star, H, Comb, and Linear Polymer Melts. *Macromolecules* **2003**, *36*, 5020−5031.

(18) Chen, W.; Zhang, K.; Liu, L.; Chen, J.; Li, Y.; An, L. Conformation and Dynamics of Individual Star in Shear Flow and Comparison with Linear and Ring Polymers. *Macromolecules* **2017**, *50*, 1236−1244.

(19) Robinson, J. W.; Zhou, Y.; Qu, J.; Erck, R.; Cosimbescu, L. Effects of Star-Shaped Poly(Alkyl Methacrylate) Arm Uniformity on Lubricant Properties. *J. Appl. Polym. Sci.* **2016**, *133*, No. 43611.

(20) Cosimbescu, L.; Robinson, J. W.; Zhou, Y.; Qu, J. Dual Functional Star Polymers for Lubricants. *RSC Adv.* **2016**, *6*, 86259−86268.

(21) Robinson, J. W.; Zhou, Y.; Bhattacharya, P.; Erck, R.; Qu, J.; Bays, J. T.; Cosimbescu, L. Probing the Molecular Design of Hyper-Branched Aryl Polyesters towards Lubricant Applications. *Sci. Rep.* **2016**, *6*, No. 18624.

(22) Van Ravensteijn, B. G. P.; Bou Zerdan, R.; Seo, D.; Cadirov, N.; Watanabe, T.; Gerbec, J. A.; Hawker, C. J.; Israelachvili, J. N.; Helgeson, M. E. Triple Function Lubricant Additives Based on Organic-Inorganic Hybrid Star Polymers: Friction Reduction, Wear Protection, and Viscosity Modification. *ACS Appl. Mater. Interfaces* **2019**, *11*, 1363−1375.

(23) Cosimbescu, L.; Malhotra, D.; Campbell, K. B.; Swita, M. S.; Kennedy, Z. C. Molecular Design and Shear Stability Correlations of Dendritic Polymethacrylates. *Mol. Syst. Des. Eng.* **2019**, *4*, 1114−1124.

(24) Van Ravensteijn, B. G. P.; Bou Zerdan, R.; Helgeson, M. E.; Hawker, C. J. Minimizing Star-Star Coupling in Cu(0)-Mediated Controlled Radical Polymerizations. *Macromolecules* **2019**, *52*, 601−609.

(25) Rubinstein, M.; Colby, R. H. *Polymer Physics*, 1st ed.; Oxford University Press Inc.: New York, 2003.

(26) ASTM D2270-04. Standard Practice for Calculating Viscosity Index from Kinematic Viscosity at 40 and 100 °C, 2004.

(27) Taylor, G. I. Stability of a Viscous Liquid Contained between Two Rotating Cylinders. *Proc. R. Soc. London, Ser. A* **1923**, *102*, 541−542.

(28) Wang, J.; Wu, C. Reexamination of the Origin of Slow Relaxation in Semidilute Polymer Solutions - Reptation Related or Not? *Macromolecules* **2016**, *49*, 3184−3191.

(29) Van Ravensteijn, B. G. P.; Vilanova, N.; De Feijter, I.; Kegel, W. K.; Voets, I. K. Temperature-Induced, Selective Assembly of Supramolecular Colloids in Water. *ACS Omega* **2017**, *2*, 1720−1730.

(30) Kline, S. R. Reduction and Analysis of SANS and USANS Data Using IGOR Pro. *J. Appl. Crystallogr.* **2006**, *39*, 895−900.

(31) SasView for Small angle scattering analysis. http://sasview.org/index.html.

(32) Guinier, A.; Fournet, G. *Small Angle Scattering of X-rays*, 1st ed.; John Wiley & Sons: New York, 1955.

(33) Hammouda, B. SANS from Homogeneous Polymer Mixtures: A Unified Overview. *Adv. Polym. Sci.* **1993**, *106*, 87−133.

(34) Birshtein, T. M.; Zhulina, E. B. Conformations of Star-Branched Macromolecules. *Polymer* **1984**, *25*, 1453−1461.

(35) Daoud, M.; Cotton, J. P. Star Shaped Polymers: A Model for the Conformation and Its Concentration Dependence. *J. Phys.* **1982**, *43*, 531−538.

(36) Winnik, M. A.; Yekta, A. Associative Polymers in Aqueous Solution. *Curr. Opin. Colloid Interface Sci.* **1997**, *2*, 424−436.

(37) Fonnum, G.; Bakke, J.; Hansen, F. K. Associative Thickeners. Part I: Synthesis, Rheology and Aggregation Behavior. *Colloid Polym. Sci.* **1993**, *271*, 380−389.

(38) Rubinstein, M.; Dobrynin, A. Solutions of Associative Polymers. *Trends Polym. Sci.* **1997**, *5*, 181−186.

(39) Campbell, K. B.; Erck, R.; Swita, M.; Cosimbescu, L. Multifunctional Tunable Polymethacrylates for Enhanced Shear Stability and Wear Prevention. *ACS Appl. Polym. Mater.* **2020**, *2*, 2839−2848.

(40) Cosimbescu, L.; Vellore, A.; Ramasamy, U. S.; Burgess, S. A.; Martini, A. Low Molecular Weight Polymethacrylates as Multi-Functional Lubricant Additives. *Eur. Polym. J.* **2018**, *104*, 39−44.

(41) Golkaram, M.; Loos, K. A Critical Approach to Polymer Dynamics in Supramolecular Polymers. *Macromolecules* **2019**, *52*, 9427−9444.

(42) Jangizehi, A.; Ahmadi, M.; Seiffert, S. Dynamics of Supra-molecular Associative Polymer Networks at the Interplay of Chain Entanglement, Transient Chain Association, and Chain-Sticker Clustering. *J. Polym. Sci., Part B: Polym. Phys.* **2019**, *57*, 1209−1223.